IEEE Photonics Journal
An IEEE Photonics Society Publication

Open Access

Effect of Carrier Leakage on Optimal AR Coatings in Midinfrared Interband Cascade Lasers

Volume 7, Number 2, April 2015

Jeyran Amirloo, Member, IEEE
Simarjeet Singh Saini, Senior Member, IEEE
Mario Dagenais, Fellow, IEEE

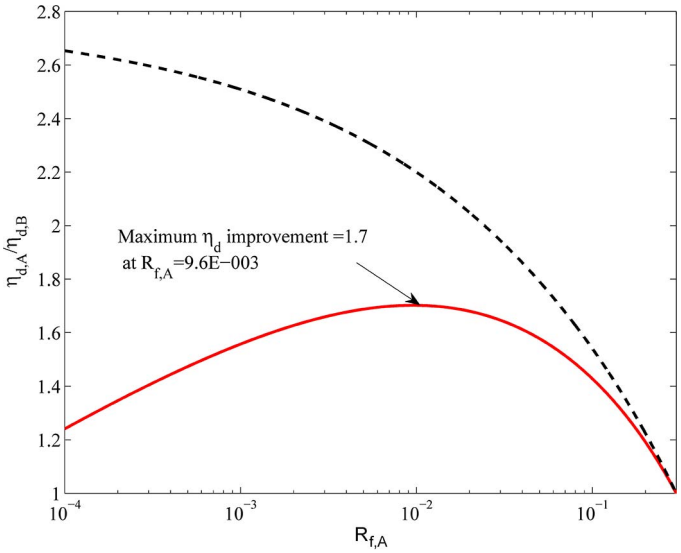

DOI: 10.1109/JPHOT.2015.2416343
1943-0655 © 2015 IEEE

IEEE photonics SOCIETY

IEEE

Effect of Carrier Leakage on Optimal AR Coatings in Midinfrared Interband Cascade Lasers

Jeyran Amirloo,[1] ***Member, IEEE*****,**
Simarjeet Singh Saini,[1,2] ***Senior Member, IEEE*****, and**
Mario Dagenais,[3] ***Fellow, IEEE***

[1]Department of Electrical and Computer Engineering, University of Waterloo, Waterloo, ON N2L 3G1, Canada
[2]Waterloo Institute of Nanotechnology, University of Waterloo, Waterloo, ON N2L 3G1, Canada
[3]Department of Electrical and Computer Engineering, University of Maryland, College Park, MD 20742 USA

DOI: 10.1109/JPHOT.2015.2416343

Manuscript received February 8, 2015; revised March 13, 2015; accepted March 19, 2015. Date of publication March 25, 2015; date of current version April 21, 2015. This work was supported through the Early Researcher Award of the Ontario Ministry of Research and Innovation. Corresponding author: M. Dagenais (e-mail: dage@ece.umd.edu).

Abstract: Variation of leakage current in interband cascade lasers (ICLs) with different carrier concentrations achieved by coating the facet with antireflections (AR) coating was experimentally studied. Single-layer Al2O3 and double-layer ZnS-YF3, ZnS-SiO2, and Ti2O5-SiO2 AR coatings are applied to midinfrared (mid-IR) ICL devices to achieve reflectance ranging from 0.15 to 7×10^{-4}. By monitoring the laser performance before and after coating, it was observed that, for lower reflectivity coatings, the leakage current appreciably rises with increasing carrier concentration, thus diminishing the slope efficiency improvements and, in fact, degrading the slope efficiency at very low reflectance. It was observed that the ratio of leakage to threshold current could increase by 17% for high carrier concentrations at very low AR coating values. The results also allow for experimental optimization of AR coatings for increased slope efficiency in mid-IR ICLs. Therefore, in this paper, we propose an optimal value for the AR coatings in order to maximize the power in ICLs.

Index Terms: Interband cascade lasers, antireflection coatings, slope efficiency.

1. Introduction

The mid-IR spectral region (3 μm to 5 μm) is comprised of two atmospheric transmission windows, as well as several absorption bands corresponding to greenhouse gasses and water. This spectral region offers applications in free space communications, sensing, and the biomedical field. Interband cascade lasers (ICL) with continuous wave (CW) room temperature (RT) power up to 500 mW [1], as well as quantum cascade lasers (QCL) [2] and type-I quantum well lasers [3], can be employed for such applications. In particular, since the original proposed ICL laser structure in 1995 [4] and the first demonstration of room temperature operation in 2008 [5], ICLs performance was continuously improved by several groups around the world [1], [6], [7].

Extensive research has been dedicated to the band structure engineering in order to increase the carrier confinement in the active quantum wells of these lasers. However, they are still

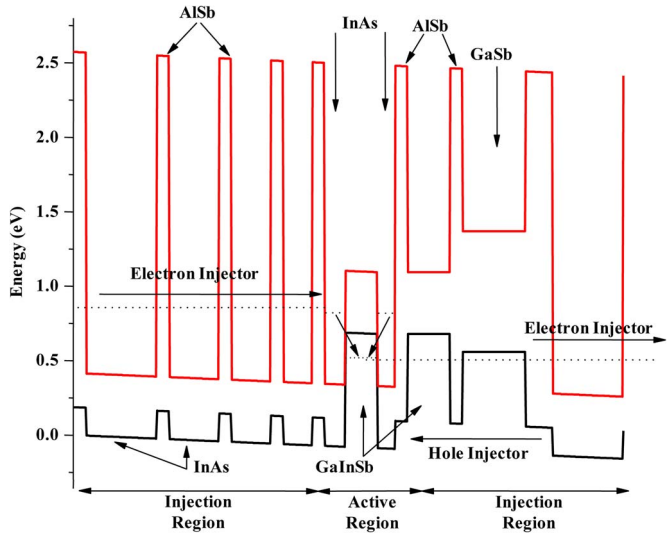

Fig. 1. Band diagram of a single stage of an ICL.

suffering from low characteristic temperatures for the threshold current and slope efficiency [1]. These issues have been attributed to non-radiative alternative paths that allow the carriers to escape to higher energy levels resulting in leakage currents. Another mechanism that contributes to temperature sensitivity of QCLs is backfilling of the lower laser level by electrons in the injector. However, this mechanism is specific to QCLs and does not play a role in ICL operation [8]. Strategies to remedy this limitation in QCLs usually involve increasing the energy level separation between the upper laser level and the next higher level in the active wells as well as between the lower laser level and the injector mini-band to decrease carrier backfilling. Deep-well [8], [9] and tapered-active-region [10], [11] QCLs are examples of these efforts. The major difference between an ICL and a QCL is that the former involves participation of both electrons and holes in the radiative transition, similar to a quantum well laser. This difference is manifest by the two orders of magnitude longer carrier lifetime in ICLs compared to QCLs and underlies why ICLs can operate with far fewer cascaded active regions [1]. ICL active region optimizations require a significant overlap between electron and hole wave functions [6]. This is in contrast to QCLs where the design focuses mostly on electron wavefunctions. This inherent difference between the two makes active region band gap engineering more challenging in ICLs [15]. Moreover, ICL has so far been limited to GaSb material systems which limits the material selection for quantum wells and barriers, again limiting the bandgap engineering that can be achieved. Therefore, implementation of similar strategies to QCLs is not as readily available in ICL structures.

The band structure of a typical ICL active region is shown in Fig. 1. At the heart of an ICL active region is a W-structure [1] that consists of one GaInSb hole-well sandwiched by InAs electron-wells. The radiative transition is a diagonal transition across the coupled electron wells and the hole well. Experimental investigation of ICLs shows high temperature dependence of the threshold current and slope efficiency [1], [12].

High power operation can be achieved by increasing the number of cascades, and/or the active area through modifying the physical dimensions of the waveguides. These approaches, however, increase the self-heating of the device in CW operation. Some of the self-heating effects could be compensated by efficient heat extraction through advance processing and packaging techniques [13]. Facet coating is another approach to enhance the output power by increasing the differential efficiency and is the focus of this study. In order to achieve higher performance through optical coating of the laser facets, the effect of the mirror reflectivity on the internal characteristics of the devices needs to be carefully examined. It is a known fact that the anti-reflection coating effectively increases the waveguide's loss and, therefore, results in a

higher threshold current. This phenomenon, consequently, raises the carrier density of the laser leading to even higher leakage current. A higher leakage reduces the internal quantum efficiency, thereby, possibly counter-balancing the positive effect of the increased mirror loss in enhancing the external slope efficiency. In fact, it has been observed for quantum cascade lasers that the slope efficiency actually decreases for low reflectivity AR coatings compared to uncoated devices [14]. Thus, optimal AR coatings need to be designed for power enhancement in IC lasers.

In this paper, we apply different levels of AR coatings with reflectivities ranging from 0.15 to 7×10^{-4} and study the performance of the ICLs in terms of an increase in threshold current, leakage current, and slope efficiency. We extract the leakage current and assess its dependence on increased carrier concentration. Our results provide an understanding of how the leakage current increases with carrier concentration within the active region and a method for optimizing the AR coatings and achieving the highest slope efficiency in ICLs.

2. AR Coating and Measurement of Reflectivity

Here, single- and multi-layer AR coatings have been applied to ridge waveguide ICLs to achieve a large range of reflectivities. Al_2O_3 single layer AR coatings and ZnS-YF_3, ZnS-SiO_2 and Ti_2O_5-SiO_2, double layer AR coatings have been applied to ICL devices resulting in a reflectance ranging from 0.15 to 7E-4. The refractive indices of these materials were measured and the coatings have been designed for the specific ICL wavelength using the simulated mode profile of the laser waveguide and plane wave decomposition technique [15]. Details of the specific thickness of the dielectric layers for the coatings are beyond the scope of this paper and will be discussed separately. The single- and multi-layer thin films were evaporated onto the facet of the device using electron-beam evaporator equipped with *in situ* reflectometry to allow for precise control over the thickness of the deposited film. The quality of dielectric layers as well as their adhesion to the substrate were tested using scanning electron microscopy and the tape test method. Further details of the AR coatings will be published separately.

In this study, 5-cascade ICL devices from three different ICL wafers were used. The wafers were grown on n-type GaSb substrate by molecular beam epitaxy (MBE) with nominally similar active structures. The 5-cascade active region is sandwiched by two 500 nm thick GaSb separate confinement regions. The upper/lower cladding layers are comprised of 1.4 μm/3 μm thick InAs/AlSb strained layer supper lattice. The structure is then capped by a heavily doped n-type InAs layer of 20 nm thickness. Electron/hole probability densities and distributions in the active region have been calculated for similar structures by Vurgaftman *et al.* [6]. The current-voltage-light (IVL) characteristics were measured before and after the coating were applied in the pulse mode with 0.05% duty cycle to avoid self-heating effects. Measurements were also done close to the threshold current where the light versus current characteristics are linear to extract the experimental parameters correctly. Threshold current and slope efficiency were extracted from the LI characteristics of the lasers. The reflectance of the applied AR coating can be extracted from the changes in the threshold current before and after the coating. Assuming a linear dependence for the threshold current density on gain [1], J_{th} of a laser can be related to mirror loss as

$$J_{th} = J_t + \frac{\alpha_m + \alpha_i}{\Gamma \frac{dg}{dj}} \tag{1}$$

where J_t is the transparency current density, α_i is the internal loss of the waveguide, α_m is the mirror loss, Γ is the optical confinement factor, and $\frac{dg}{dj}$ is the differential gain per unit current density at transparency. The mirror loss is defined as

$$\alpha_m = \frac{1}{2L} ln \frac{1}{R_f R_b} \tag{2}$$

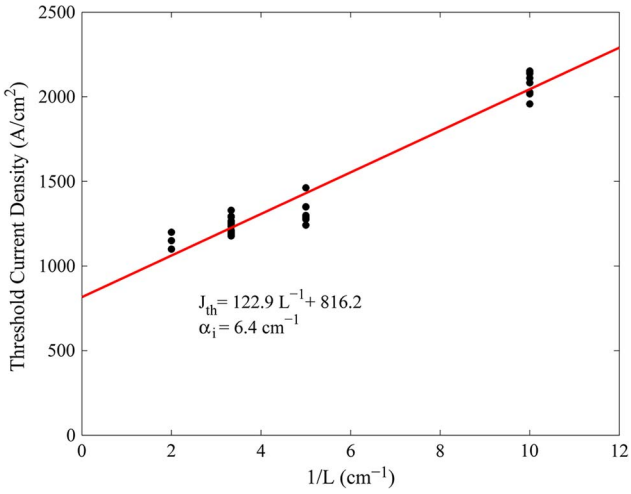

Fig. 2. Length dependent analysis of the ICL-3 which has been carried out for five different lengths of 1 mm, 2 mm, 3 mm, and 5 mm.

where L is the cavity length and R_f and R_b are the front and back facet power reflectivity coefficients, respectively. We have previously shown that J_t is negligible compared to $\alpha_i\Gamma(dg/dj)$ in ICLs [12]. Equation (1) can then be approximated as

$$J_{th} = \frac{\alpha_i + \alpha_m}{\Gamma\frac{dg}{dj}} = \frac{1}{\Gamma\frac{dg}{dj}}\left(\alpha_i + \frac{1}{2L}ln\frac{1}{R_f R_b}\right). \tag{3}$$

The AR coating reflectivity can then be extracted by comparing the threshold current before and after the coating

$$\frac{J_{th,A}}{J_{th,B}} = \frac{\alpha_{m,A} + \alpha_i}{\alpha_{m,B} + \alpha_i} \tag{4}$$

where the subscript A and B refer to the parameter values after and before the coating is applied. In order to extract $\alpha_{m,A}$ after the coating, one needs to know α_i accurately. As can be seen in equation (3), J_{th} and L^{-1} have a linear relationship that can be deduced by a cavity length analysis through measuring several un-coated devices, with at least three different lengths. The ratio of the intercept to the slope of the graph multiplied by $ln(1/R)$ gives the value of α_i where R is the reflectivity of the uncoated facet. Thus, two separate experiments were conducted to extract the reflectivity of the coatings. One is a cavity length analysis to extract α_i using multiple lengths and, second, comparing the threshold current densities before and after coating. Fig. 2 shows a typical example of the cavity length analysis. The length dependent analysis for each of these ICLs has been carried out with 3–5 different lengths and more than 20 devices per length. These devices are ridge waveguides with a 12 μm width and etch depth of 3 μm that were cleaved in various lengths varying from 1 mm to 5 mm and measured in the pulse mode to minimize self-heating effects. The processing steps for fabricating these ICLs have been detailed elsewhere [12]. The J_{th} and L^{-1} relation for all of these samples, as well as the internal loss and the emission wavelengths, are summarized in Table 1.

An example for the LIV characteristics used in the extraction process is shown in Fig. 3. For this specific example, the AR coating was designed for 2% reflectivity using ZnS-SiO_2 to ICL-2 (details are discussed below). This coating resulted in the highest improvement of slope efficiency by a factor of 1.95. The threshold current density was increased by 49%. We also monitored the VI characteristics of the device before and after the coating and if the VI

TABLE 1

Internal loss, wavelength of emission, and cavity length dependence of threshold current for the ICLs that have been used in this study

ICL Material	Threshold Current Density [A/cm^2] vs. inverse cavity length [cm^{-1}]	α_i[cm^{-1}]	λ [μm]
ICL-1	J_{th}=34.90L^{-1}+208.9	5.8	3.4
ICL-2	J_{th}=43.26L^{-1}+221.3	4.9	3.8
ICL-3	J_{th}=122.9L^{-1}+816.2	6.4	3.5

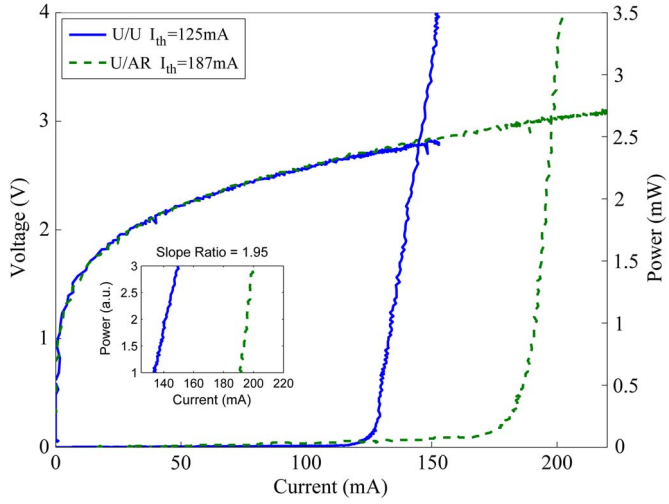

Fig. 3. LIV characteristics before and after ZnS-SiO_2 double layer AR coating at 150 °C for a 3 mm ICL-2. Internal parameters were extracted from change in slope and threshold currents.

characteristics changes, the coating was considered to have affected the diode characteristics and was not considered good.

In order to span a wide range of reflectivity with the simplest coating combination, materials close to the optimum refractive index for the AR coating were considered. For an ICL ridge waveguide with a width of 12 μm and a height of 3 μm and a waveguide effective index of $\sim$3.5, the optimum single layer coating should have an index of refraction equal to 1.87, i.e. the geometric mean of the effective refractive index of the waveguide and air. However, considering the material limitation it is not possible to match this ideal value. Consequently, the available material close to this index, Al_2O_3, was selected. For double layer coating two materials with high and low refractive indices are required. While choices for a low index material are relatively broad, there are only a few high index materials that are suitable for optical coatings in the mid-infrared region that possess the required index difference with the substrate. Given the optimal refractive indices for a double layer coating, $\sqrt{(1/3)(n_s n_a)}$ and $\sqrt{(2/3)(n_s n_a)}$, the following materials were considered for the high index layer:

- ZnS with index of 2.26 in the infrared region;
- TiO_2 with the index of 1.77 in the infrared region.

For low index layers YF_3 and SiO_2 with the index of $\sim$1.4 in the infrared region were used. Table 2 lists the dielectric materials that have been used as well as their approximate refractive indices at Mid-IR. These indices were estimated though fitting Sellmeier equation to ellipsometry measurements on the witness samples at shorter wavelengths. The witness samples are placed in the same E-beam evaporation chamber where the actual AR coating took place.

TABLE 2

Thin-film dielectrics and their measured refractive indices

Dielectric Materials	Approximate Index of Refraction at Mid-IR
Al_2O_3	1.5
ZnS	2.26
TiO_2	1.77
SiO_2	1.46
YF_3	1.4

TABLE 3

Summary of AR coating experiments

AR coating material combination	*ICL Material*	*L* [cm]	α_i[cm^{-1}]	$I_{th,A}/I_{th,B}$	$R_{f,A}$
Al_2O_3	ICL-1	0.1	5.8	1.25	0.12
YF_3-ZnS	ICL-3	0.1	6.4	1.48	0.05
(Ta_2O_5) ZnS-YF_3	ICL-3	0.2	6.4	1.35	0.05
TiO2 –SiO2	ICL-1	0.1	5.8	1.41	0.06
(Ta_2O_5) ZnS-SiO_2	ICL-2	0.3	4.9	1.49	0.02
(Ta_2O_5) ZnS-SiO_2	ICL-1	0.1	5.8	2.6	7.2E-4

Six different AR coatings with reflectivity ranging from 0.12 to 7×10^{-4} were studied. Table 3 summarizes the ratio of the change in the threshold current before and after anti-reflection coating, the length of the particular device and its internal loss extracted from the length dependent measurement as well as reflectivity of the coating extracted from the change in the threshold current according to equation (4). Each combination was designed to reach a certain reflectivity with the exception of (Ta_2O_5) ZnS-SiO_2 double layer coating. This material combination was used in two different thickness combinations, one was designed to achieve moderately low reflectivity of 2% and the other was designed for a reflectivity equal to 7×10^{-4}.

3. Extraction of Leakage Current

Leakage current was extracted from the slope efficiency calculations. The differential quantum efficiency is also related to the facet reflectivity via:

$$\eta_d = F_f \eta_i N \frac{\alpha_m}{\alpha_m + \alpha_i} \tag{5}$$

where η_i is the differential internal efficiency per stage; N is the number of stages, which is equal to 5 in this case; and F_f is the fraction of total output power delivered from the front facet, determined by both facet reflectivities and is given by [16]

$$F_f = \frac{1 - R_f}{(1 - R_f) + \sqrt{\frac{R_f}{R_b}}(1 - R_b)}. \tag{6}$$

The modification of facet reflectivities affects the slope efficiency by changing F_f and α_m. Furthermore, due to the increase in carrier concentration leading to higher leakage current, η_i can also reduce appreciably. The differential internal efficiency is a measure of the fraction of the total current above the threshold that results in carrier generation in the active region. By using a

four-level system, Botez *et al.* [8], [17] expressed η_i in terms of the differential pumping efficiency η_p and the laser transition differential efficiency η_{tr} [18] as

$$\eta_i = \eta_{tr}\eta_p = \eta_{tr}\left(1 - \frac{J_{leak,th}}{J_{th}}\right) \tag{7}$$

where $J_{leak,th}$ is the leakage current density, and J_{th} is the threshold current density.

It is this leakage current which is attributed to the high temperature sensitivity of the threshold current density and slope efficiency of ICLs. The low characteristic temperature of the threshold current and the slope efficiency, T_0 and T_1, respectively, indicate a sizable contribution from the carrier leakage. We have previously reported T_1 to be approximately 90 K [19]. Though the leakage current did not explicitly appear in equation (1) for threshold current, it can be easily shown that it is indeed part of the threshold current density. Using $J = (q/\eta_i'\tau)n$, where n is the carrier concentration and η_i' is the internal efficiency, (1) becomes

$$J_{th} = \frac{q}{\eta_i'\tau}\left[n_t + \frac{\alpha_m + \alpha_i}{\Gamma\frac{dg}{dn}}\right]. \tag{8}$$

Substituting the value of $\eta_i' = \eta_{inj}\eta_p \approx \eta_p$ in (8), where η_{inj} is the carrier injection efficiency, gives

$$J_{th} = \frac{q}{\tau}\left[n_t + \frac{\alpha_m + \alpha_i}{\Gamma\frac{dg}{dn}}\right] + J_{leak}. \tag{9}$$

Thus, the linear approximation of gain to threshold current density in (1) accounts for the leakage current within its formulation.

The same leakage current can also play an important role in the case of AR coated devices. Due to a considerable increase in the threshold current density, particularly at very low reflectivity, the threshold carrier density before and after coating changes dramatically which in turn affects the internal device parameters.

Using (5), the change in the differential quantum efficiency is related to the internal laser parameters by

$$\frac{\eta_{d,A}}{\eta_{d,B}} = \frac{F_{f,A}\eta_{p,A}\frac{\alpha_{m,A}}{\alpha_{m,A}+\alpha_i}}{F_{f,B}\eta_{p,B}\frac{\alpha_{m,B}}{\alpha_{m,B}+\alpha_i}} \tag{10}$$

where F_f, α_m are obtained from the reflectivity in Table 3. A and B subscripts correspond to values after and before coatings respectively. From (10), $(\eta_{p,A}/\eta_{p,B})$ is calculated which is the ratio of differential pumping efficiency after and before the AR coatings. In this calculation, it is assumed that the laser transition differential efficiency η_{tr} does not change in the process. The laser transition differential efficiency is not temperature dependent and is not expected to change with AR coatings significantly either.

In order to obtain the value of the leakage current, the absolute value of the uncoated laser internal differential efficiency is required. η_i can be calculated using the calibrated slope efficiency from

$$\frac{dP}{dI} = \frac{h\nu}{2q}\eta_i N\frac{\alpha_m}{\alpha_m + \alpha_i}. \tag{11}$$

We have estimated η_i to be 30.6% for our lasers in a previous study [19], mainly limited by the leakage current. Using the initial value of internal efficiency for uncoated device, and the change of the internal efficiency from (10), the final η_i after coating is obtained. The threshold current densities before and after the coating are then inserted in (7) to obtain the leakage current with the additional assumption that the η_{tr} is unity. Here, it is important to note that the initial value of η_i and the contribution from the transition efficiency will solely effects the ratio of the leakage

TABLE 4

Summary of the extracted reflectivities, the ratio of slope efficiency, internal differential efficiency threshold current, and leakage current after and before the AR coating is applied

AR coating material combination	$R_{f,A}$	L [cm]	$\eta_{d,A}/\eta_{d,B}$	$\eta_{i,A}/\eta_{i,B}$	$I_{th,A}/I_{th,B}$	$(I_{leak,A}/I_{thA})$	$(I_{leak,A}/I_{thA})/(I_{leak,B}/I_{thB})$
Al_2O_3	0.12	0.1	1.33	0.91	1.25	0.72	1.03
YF_3-ZnS	0.05	0.1	1.5	0.83	1.48	0.74	1.07
(Ta_2O_5) ZnS-YF_3	0.05	0.2	1.5	0.76	1.35	0.76	1.10
TiO_2 –SiO_2	0.06	0.1	1.47	0.85	1.41	0.73	1.06
(Ta_2O_5) ZnS-SiO_2	0.02	0.3	1.95	0.81	1.49	0.75	1.08
(Ta_2O_5) ZnS-SiO_2	7.2×10^{-4}	0.1	1.7	0.67	2.6	0.79	1.17

current to threshold current before and after the application of AR coating. The ratio of the internal efficiency and subsequent optimization of anti-reflection coating is independent of these assumptions. The extracted values of the ratio of the differential efficiencies; internal differential efficiencies and leakage currents after and before are summarized in Table 4.

4. Discussion

As seen from the Table 4, the ratio of the differential efficiency before and after coating increases with reduced facet reflectivity up to 2% (as is expected) but then decreases for the lowest reflectivity of 7×10^{-4}. Similar results have been previously seen in AR coatings on QCLs where the slope efficiency decreased at very low reflectivity [14], [20]. In fact, in their experiment, the slope efficiency for low reflectivity of 1E-4 was lower than that of a laser with uncoated facet [20]. The reason for this degradation lies in the change of the internal efficiency as seen from the data in Table 4. The degradation in the differential internal efficiency, η_i, before and after coating worsens as the reflectivity of the facet reduces. The improvement of the differential efficiency resulting from lowering the mirror loss compensates only part of the degradation of internal efficiency caused by the increased carrier concentration. The relationship between the ratios of the internal efficiency after and before coating as a function of the reflectivity of the facet is plotted in Fig. 4. The internal efficiency ratio changes logarithmically with reducing the facet reflectivity indicating a more drastic change for ultra-low reflectivities. The decrease in the internal differential efficiency results from a substantial increase in the leakage current as larger proportions of the carriers are leaking at lower reflectivity as compared to the uncoated facet situation. The results also show how the leakage current increases as the carrier concentration increases in the active region. The initial value of internal efficiency is required to calculate the ratio of leakage current to the threshold current and its change with the mirror loss. For an internal efficiency of 30.6% and laser transition efficiency of unity, the leakage to threshold current ratio increased by as much as 17% by increasing the mirror with low reflectivity AR coated samples. However, the trend of increase in the leakage current and the ratio of the internal efficiency are of greater importance.

This leakage current is attributed to the thermal excitation of the injected electrons to higher energy levels in the active region. Electrons in these higher energy levels can either relax to lower energy levels or escape to continuum. The barrier height in the active and injection region play an essential role in determining the leakage current in ICLs.

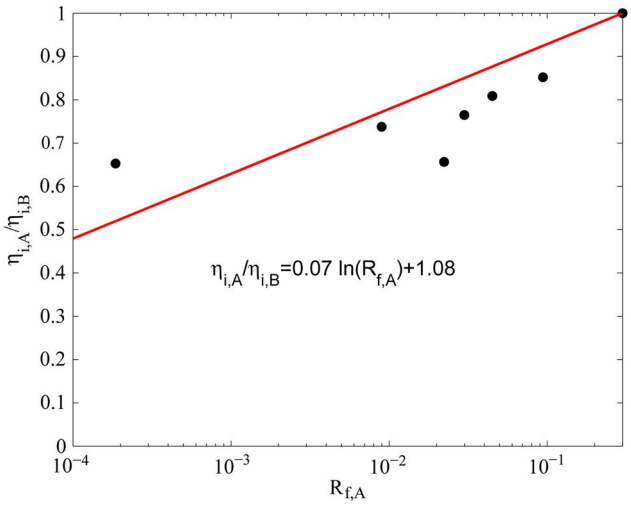

Fig. 4. Ratio of internal differential efficiency after and before the coatings $(\eta_{i,A}/\eta_{i,B})$ as the facet reflectivity is changed.

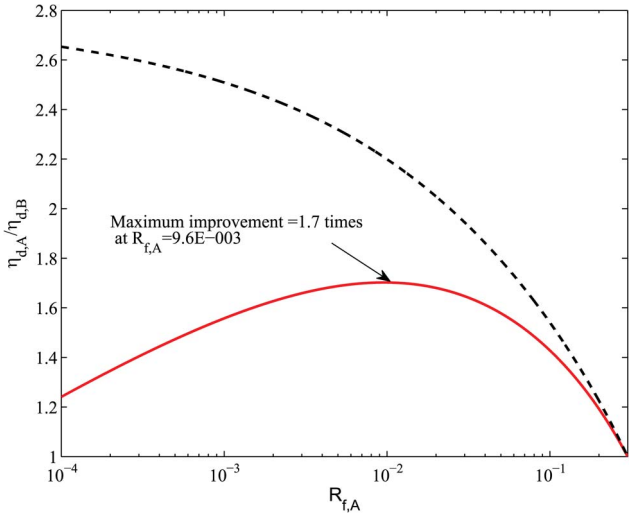

Fig. 5. Ratio of differential quantum efficiencies vs. Reflectivity considering the decrease in the internal diffrential efficiency (solid line). Ratio of differential quantum efficiencies vs. Reflectivity is also plotted for constant internal differential efficiency (dashed-line) for comparison.

These results suggests that the optimization procedure for designing the anti-reflection coatings for achieving the highest differential efficiency must take into account the introduction of additional leakage in the device. For high power applications where maximum differential efficiency is required, very low reflectivities can be counterproductive as they result in substantial increase in the leakage current and degrade the device performance. The increase in the leakage current would in turn decrease the differential efficiency resulting in a less-efficient device.

In order to visualize such dependencies, the ratio slope efficiency was calculated for a 1 mm device with internal loss of 6 cm^{-1}, using the fitted logarithmic function for internal efficiency. For comparison, the ratio of the slope efficiency was also calculated for the same device assuming a constant internal efficiency. The results for both scenarios are plotted in Fig. 5. As can be seen from this plot, the slope efficiency improves at first by lowering the reflectivity but starts to

decrease as the reflectivity is further lowered. For this particular case, the maximum slope efficiency improvement is 1.7 times and is obtained at a front facet reflectivity of ~1%. It should be noted that this value changes for different device lengths and depends on the internal loss. High reflectivity coating of the back facet is also recommended and would allow for higher improvement with lower reflectivities.

5. Conclusion

In conclusion, this study shows how the leakage current increases with carrier concentration in the active region and the resulting reduction of the internal efficiencies limits the improvement of the slope efficiency with AR coatings. While the reduction of the front facet reflectivity allows for higher output power, the cost of increasing the carrier density has to be accounted for in order to find the optimum balance. If other laser parameters are also affected, for example, if the internal loss increases as a result of the increase in carrier density, there could be a further reduction of the slope efficiency after a certain point in lowering the facet reflectivity. These changes are expected to be small compared to the effective loss associated with carrier leakage.

Based on our previous findings and similar works on Mid-IR QCL, the relatively low characteristic temperature of the threshold current density and the slope efficiency in the semiconductor lasing materials are linked to carrier leakage from the active quantum wells. The results of the anti-reflection coating also indicate the sensitivity of these devices to the number of carriers in the active region. Better carrier confinement in QCLs through application of high barriers and tapered injectors [8], [10] has led to substantial improvement in QCL performance at room and high temperatures. Future work should focus on implementing similar ideas for ICLs to improve their performance and stability. We expect a substantial improvement in the wall-plug efficiency and in the amount of power that can be extracted from ICL lasers by appreciably reducing the carrier leakage in these lasers.

Acknowledgment

The authors would like to extend their gratitude to Dr. J. Bruno and F. Towner for supplying the samples used in this study.

References

[1] I. Vurgaftman *et al.,* "Interband cascade lasers with low threshold powers and high output powers," *IEEE J. Sel. Topics Quantum Electron.*, vol. 19, no. 4, Jul./Aug. 2013, Art. ID. 1200210.
[2] A. Lyakh, R. Maulini, A. Tsekoun, R. Go, and C. K. N. Patel, "Tapered 4.7 μm quantum cascade lasers with highly strained active region composition delivering over 4.5 watts of continuous wave optical power," *Opt. Exp.*, vol. 20, no. 4, pp. 4382–4388, 2012.
[3] T. Hosoda, G. Kipshidze, L. Shterengas, and G. Belenky, "Diode lasers emitting near 3.44 μm in continuous-wave regime at 300 K," *Electron. Lett.*, vol. 46, no. 21, pp. 1455–1457, Oct. 2010.
[4] R. Q. Yang, "Infrared laser based on intersubband transitions in quantum wells," *Superlattices Microstruct.*, vol. 17, no. 1, pp. 77–83, Jan. 1995.
[5] M. Kim *et al.,* "Interband cascade laser emitting at $\lambda = 3.75$ μm in continuous wave above room temperature," *Appl. Phys. Lett.*, vol. 92, no. 19, May 2008, Art. ID. 191110.
[6] I. Vurgaftman *et al.,* "Rebalancing of internally generated carriers for mid-infrared interband cascade lasers with very low power consumption," *Nat. Commun.*, vol. 2, no. 12, p. 585, Dec. 2011.
[7] R. Weih, M. Kamp, and S. Hofling, "Interband cascade lasers with room-temperature threshold current densities below 100 A/cm^2," *Appl. Phys. Lett.*, vol. 102, no. 23, Jun. 2013, Art. ID. 231123.
[8] D. Botez *et al.,* "Electron leakage and its suppression via deep-well structures in 4.5-to 5.0-μm-emitting quantum cascade lasers," *Opt. Eng.*, vol. 49, no. 11, Nov. 2010, Art. ID. 111108.
[9] D. Botez *et al.,* "Temperature dependence of the key electro-optical characteristics for midinfrared emitting quantum cascade lasers," *Appl. Phys. Lett.*, 97, no. 7, Aug. 2010, Art. ID. 071101.
[10] J. D. Kirch *et al.,* "Tapered active-region quantum cascade lasers $(\lambda = 4.8$ μm$)$ for virtual suppression of carrier-leakage currents," *Electron. Lett.*, vol. 48, no. 4, 234–235, Feb. 2012.
[11] Y. Bai *et al.,* "Highly temperature insensitive quantum cascade lasers," *Appl. Phys. Lett.*, vol. 97, no. 25, Dec. 2010, Art. ID. 251104.
[12] G. Ryu *et al.,* "Gain and losses and room-temperature operation in interband cascade lasers," *IEEE Photon. J.*, vol. 4, no. 1, 133–142, Feb. 2012.

[13] A. Chryssis, G. Ryu, and M. Dagenais, "Thermal impedence of epi-up and epi-down interband cascade lasers," in *Proc. 23rd Annu. Meeting IEEE Photon. Soc.*, 2010, pp. 421–422.
[14] R. Maulini *et al.,* "High power thermoelectrically cooled and uncooled quantum cascade lasers with optimized reflectivity facet coatings," *Appl. Phys. Lett.*, vol. 95, no. 15, Oct. 2009, Art. ID. 151112.
[15] A. N. Chryssis, "Design and Fabrication of High-Performance Interband Cascade Tunable External Cavity Lasers," Ph.D. dissertation, Dept. Elect. Eng., Univ. Maryland, College Park, MD, USA, 2011.
[16] L. A. Coldren, S. W. Corzine, and M. L. Mashanovitch, *Diode Lasers and Photonic Integrated Circuits*, vol. 218. Hoboken, NJ, USA: Wiley, 2012.
[17] D. Botez *et al.,* "Multidimensional conduction-band engineering for maximizing the continuous-wave (CW) wallplug efficiencies of mid-infrared quantum cascade lasers," *IEEE J. Sel. Topics Quantum Electron*, vol. 19, no. 4, Jul./Aug. 2013, Art. ID. 1200312
[18] J. Faist, "Wallplug efficiency of quantum cascade lasers: Critical parameters and fundamental limits," *Appl. Phys. Lett.*, vol. 90, no. 25, Jun. 2007, Art. ID. 253512
[19] J. Amirloo, F. J. Towner, S. Saini, and M. Dagenais, "Carrier leakage in interband cascade lasers," in *Proc. 23rd IEEE ISLC*, 2012, pp. 130–132.
[20] R. Maulini, "Broadly tunable mid-infrared quantum cascade lasers for spectroscopic applications," Ph.D. dissertation, Inst. Phys., Univ. Neuchatel, Switzerland, 2006.